RSC Advances

PAPER

View Article Online
View Journal | View Issue



Cite this: *RSC Adv.*, 2017, **7**, 27162

# Overcoming the blood–brain barrier for glioma-targeted therapy based on an interleukin-6 receptor-mediated micelle system†

Wei Shi,[b] Xuexue Cui,[a] Jinlong Shi,[b] Jian Chen[b] and Yi Wang *[ac]

Treatments of cancer in the central nervous system (CNS), such as glioma, require nano-drugs to efficiently cross the blood–brain barrier (BBB) and highly accumulate within tumor regions. In this work, a new interleukin-6 receptor-mediated micelle system, where a short peptide $I_6P_8$ was conjugated to biodegradable poly(ethylene glycol)–poly(lactic-*co*-glycolic acid) (PEG–PLGA), was prepared for cascade-targeting drug delivery to glioma. *In vitro* results showed that the $I_6P_8$-conjugated doxorubicin (DOX)-loaded micelle ($I_6P_8$-D-M) could significantly transport across the BBB and subsequently target the glioma cells, which was superior to results of scrambled peptide-modified counterparts. While *in vivo* results confirmed that this multifunctional $I_6P_8$-D-M could introduce the highest glioma apoptosis and longest survival of glioma-bearing mice as compared to other groups. These findings suggest that the $I_6P_8$-D-M micelle system is a promising cascade-targeting therapeutic agent, which can overcome the BBB for glioma-targeted therapy.

Received 18th March 2017
Accepted 13th May 2017

DOI: 10.1039/c7ra03208k

rsc.li/rsc-advances



## 1. Introduction

Effective delivery of therapeutic agents to the target sites is a promising strategy for treatments of different diseases, especially refractory cancers. Targeting technologies, including enhanced permeation and retention (EPR) effect-based passive targeting and ligand-mediated active targeting, are used to guide the therapeutic cargos to specific regions for the targeting therapy.[1,2] However, for the treatments of central nervous system (CNS) diseases, such as malignant brain tumors (glioma), the simple passive or active tumor-targeted strategies are inadequate in delivering therapeutic agents to the desired locations. On one hand, for glioma, even in the late stage, passive accumulation of nanoparticles is not as characteristic as that in other solid tumors.[3,4] Drug delivery has been reported to be less efficient in cranial tumors than that in subcutaneous ones.[3,4] Thus drug delivery systems with small sizes such as micelles have more potential for glioma therapy.[5,6] On the other hand, the presence of blood–brain barrier (BBB), which is a unique physiological interface between the CNS and the systemic blood circulation, can strictly restrict the transmembrane transport of substances into the brain.[7,8] To overcome the BBB, elaborate strategies, including penetration *via* intracranial injection, BBB disruption *via* chemical or physical approaches, and transportation *via* biological regulations, have been employed for brain drug delivery.[7,9–12] Among them, traversing BBB mediated by biological molecules (proteins, peptides, *etc.*) has been recognized as the most prospective technology due to its high bioactivity, low invasion and good biosafety.[7,13,14] Therefore, combination of biological molecule-mediated BBB traversing and ligand-mediated active targeting would favor the successful brain drug delivery. Nevertheless, the current prevalent strategies for this aim mainly focus on the mediation *via* dual agents (one biological molecule and one ligand), which consequently increase the complexity, decrease the stability and compromise the targeting ability.[15–17] Single biological agent-mediated cascade-targeting strategy across the BBB and then accumulating within glioma may alleviate those drawbacks to dual mediation, which is thereupon subjected to the multiplicity of the biological agents. The main concern for this purpose is the common target in both BBB and glioma cells.

Recently, interleukin 6 receptor (IL-6R) has been reported to be overexpressed on glioma cells and also on the BBB, while almost not on healthy astrocytes.[18] The natural ligand of IL-6R, IL-6, was firstly considered as the cascade-targeting ligand. Unfortunately, the interaction between IL-6R and IL-6 facilitates the glioma growth, as introduced by autocrine growth promotion and angiogenesis induction *via* activation of vascular epithelial growth factor A (VEGF-A).[18] Thus, IL-6 can not be used as the targeting ligand for glioma drug delivery. Furthermore, blocking IL-6R could inhibit the IL-6R/IL-6 interaction and

[a]*Center for Advanced Low-dimension Materials, Donghua University, Shanghai 201620, China. E-mail: ywang@dhu.edu.cn*

[b]*Department of Neurosurgery, Affiliated Hospital of Nantong University, Nantong 226001, China*

[c]*Center of Analysis and Measurement, Fudan University, Shanghai 200433, China*

† Electronic supplementary information (ESI) available. See DOI: 10.1039/c7ra03208k

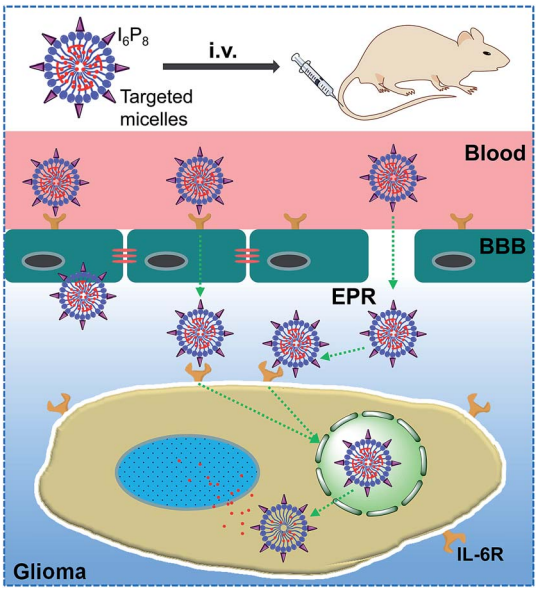


Scheme 1 Transportation of targeted micelles after intravenously injected to glioma-bearing mice.

further inhibit the glioma growth,[18,19] suggesting that IL-6R represents a potential target for both therapy and glioma-targeted delivery across the BBB.

By phage display, a short peptide ligand, LSLITRL, was reported to possess similar targeting function for selectively binding with IL-6R to mediate nanoparticles into glioma cells,[19] inhibiting the tumor growth.[18] More importantly, this peptide could also inhibit tumor growth by the competitive binding with IL-6R as an IL-6 antagonist.[18–20] Therefore, an N-terminally cysteinized LSLITRL, $I_6P_8$ peptide, would be considered to be a significant cascade-targeting ligand for glioma-targeted drug delivery across the BBB, and at the same time a therapeutic agent against glioma growth.

In this work, an canonical polymeric drug carrier, biodegradable poly(ethylene glycol)–poly(lactic-*co*-glycolic acid) (PEG–PLGA) micelle, which has been proved to be an robust vehicle for long-term delivery of BBB impermeable therapeutic agents to tumor, was modified by $I_6P_8$ peptide, and then deliver hydrophobic anticancer drug doxorubicin (DOX) to overcome the BBB for glioma-targeted therapy. The constructed brain drug delivery system, systematically demonstrated *in vitro* and *in vivo*, was illustrated in Scheme 1.

# 2. Experimental section

## 2.1. Materials

Mal–$PEG_{5.5k}$-*b*-PLGA $(75:25)_{2.2k}$ and $mPEG_{4k}$-*b*-PLGA $(75:25)_{2.2k}$ were purchased from Advanced Polymer Materials Inc. (Montreal, Canada). Targeting $I_6P_8$ peptide and scrambled $I_6P_8$ peptide ($I_6P_8$scr) were synthesized by Ziyu Biotech (Shanghai, China). DOX was bought from Huafeng United Tech (Beijing, China). TdT-mediated dUTP nick end labeling (TUNEL) apoptosis detection kit (FITC-labeled) was purchased from Keygen Biotech (Nanjing, China). Temozolomide (TMZ) was purchased from Meilun Biotech (Dalian, Chain). Trimethylamine (TEA), sodium fluorescein (NaF), indocyanine green (ICG), and other reagents, if not specified, were obtained from Sigma-Aldrich (MO, U.S.A.). All the chemicals were used without further purification.

Brain endothelial bEnd.3 cells were bought from ATCC (MD, U.S.A.). Human glioma U251 cells were purchased from Shanghai Cell Bank, Chinese Academy of Medical Sciences. U251 cells stably expressing green fluorescent proteins (GFP-U251 cells) were obtained from Genomeditech (Shanghai, China). Rat astrocytes (RA) cells were obtained from ScienCell Research Laboratories.

## 2.2. Synthesis and characterization of different polymers

$I_6P_8$ and its scrambled peptide were conjugated to Mal–PEG–PLGA based on the specific reaction of thiol group (–SH) in cysteine of peptides and maleimide group (–Mal) in the polymer. Peptides (1 mg) and Mal–PEG–PLGA (9.5 mg) were dissolved in PBS (pH 7.0) at the molar ration of 1.2 : 1 and stirred at room temperature overnight. Then the products were purified *via* dialysis against distilled water (MWCO = 10 000). The resulting peptide-conjugated polymers ($I_6P_8$–PEG–PLGA and $I_6P_8$scr–PEG–PLGA) were freeze-dried and stored for further usage.

To characterize the synthesis, different polymers were dissolved in deuterium chloroform and characterized using a 400 MHz nuclear magnetic resonance (NMR) spectrometer (Varian, USA).

## 2.3. Preparation of different micelles

Different DOX-loaded micelles were prepared using thin film rehydration method mainly as described previously.[21] Briefly, 2 mg DOX was dispersed in 6 ml acetonitrile and excessive TEA (30 μl) was added to discard hydrochloric acid. And, different amount of $I_6P_8$–PEG–PLGA and mPEG–PLGA (the initial amount was 4 mg) with the molar percent of $I_6P_8$–PEG–PLGA ranged from 0% to 40% were mixed and dissolved in 4 ml acetonitrile. Then DOX was added at a molar ratio of 6 : 1 to total PEG–PLGA. After that the mixture was rotarily evaporated at 60 °C and then the obtained thin film was hydrated with saline. Unencapsulated DOX was removed *via* ultrafiltration and detected using a fluorescence spectrophotometer (Cary Eclipse, Agilent, U.S.A.).

## 2.4. Characterizations of micelles

Drug encapsulation efficiency (EE) and loading content (LC) were calculated as follows.

$$\mathrm{EE}(\%) = \frac{\text{weight of DOX in micelles}}{\text{weight of the feeding DOX}} \times 100\%$$

$$\mathrm{LC}(\%) = \frac{\text{weight of DOX in micelles}}{\text{weight of DOX-loaded micelles}} \times 100\%$$

The sizes of different micelles were measured by a dynamic light scattering using a Nano-ZS instrument (Malvern, UK). Corresponding polydispersity was also recorded.

### 2.5. Cell culture

Human glioma U251 cells were cultured in special Dulbecco's modified Eagle medium (DMEM) supplemented with 10% fetal bovine serum (FBS), 1% L-glutamine, 1% penicillin and 1% streptomycin, at 37 °C and in 5% $CO_2$ atmosphere. The GFP-U251 cells were cultured at the similar condition with U251 cells, except the addition of 15% FBS.

Brain capillary endothelial cells (bEnd.3) were expanded and routinely cultured in DMEM with the addition of 20% heat-inactivated FBS, 100 μg $ml^{-1}$ epidermal cell growth factor (ECGF), 2 mM L-glutamine, 40 U $ml^{-1}$ heparin, 100 U $ml^{-1}$ penicillin, 100 μg $ml^{-1}$ streptomycin, and maintained at 37 °C under a humidified atmosphere containing 5% $CO_2$. RA cells were cultured under the same condition as bEnd.3.

### 2.6. Cellular uptake

To optimize the molar percent of $I_6P_8$–PEG–PLGA, confocal microscopy and intracellular DOX level were performed to qualify and quantify the cellular uptake levels, respectively. U251 cells were seeded in 96-well microplates at a density of $1 \times 10^4$ cells per well for 24 h. DOX-loaded micelles (calculated DOX concentration was 100 μg $ml^{-1}$) with the molar percent of $I_6P_8$–PEG–PLGA ranged from 0% to 40% were incubated with U251 cells for 1 h. Then the cells were rinsed with PBS and fixed with 4% paraformaldehyde for 15 min, after which the medium was changed to PBS. Confocal microscopy was performed using a TCs SP5 microscope (Leica, Germany). For quantitative evaluation, U251 cells were seeded in 24-well plates at a density of $5 \times 10^4$ cells per well for 24 h, then incubated with DOX-loaded micelles (calculated DOX concentration was 100 μg $ml^{-1}$) with the molar percent of $I_6P_8$–PEG–PLGA ranged from 0% to 40% for 1 h. After that, cells were rinsed with PBS three times, lysed with 1% triton (200 μl per well), and the protein level was determined using the Bio-Rad Protein Assay Kit.[22] The intracellular DOX level was measured by a fluorescence spectrophotometer. And the calculated DOX concentrations to cell proteins were used for evaluation.

### 2.7. Transportation studies in BBB monolayers

*In vitro* BBB monolayers were constructed in a modified method according to our previous work.[13] Briefly, bEnd.3 cells were seeded in 24-well transwell filters (Falcon Cell Culture Insert, Becton Dickinson Labware, NJ, U.S.A.) at a density of $6 \times 10^4$ cells per $cm^2$. One week later, confluency was verified under a microscope, and the transendothelial electrical resistance (TEER) was measured to monitor the BBB monolayer integrity *via* an epithelial voltohmmeter. Only BBB monolayers with TEER larger than 200 Ω $cm^2$ were used for transportation studies. Furthermore, NaF with final concentration of 10 μg $ml^{-1}$ was used as an indicator to monitor the BBB monolayer integrity during the entire experiment.

Different DOX-loaded micelles (100 μl) were added in the donor chamber of the transwells with the addition of NaF. The accepter chamber contained 900 μl Hank's solution. The wells were incubated at 37 °C under 50 rpm shaking condition. An aliquote of 300 μl sample was removed from the acceptor chamber and the same volume of fresh medium was added back immediately at 5, 10, 15, 30, 45 and 60 min. The transported amount of DOX was determined using a Tecan Infinite M1000 Pro microplate reader (Switzerland). The apparent permeability ($P_{app}$) was calculated as follows:[13]

$$P_{app} = \frac{\partial Q}{\partial t C_0 A}$$

where $\partial Q/\partial t$ represents the permeability rate (nmol $s^{-1}$), $C_0$ is the initial concentration (nmol $ml^{-1}$) in the donor chamber, and $A$ is the surface area ($cm^2$) of the filter membrane. The data of transport ratio of micelles were also presented.

### 2.8. Targeting evaluation *in vitro*

*In vitro* glioma-targeted efficiency of different micelles was evaluated using confocal microscopy. GFP-U251 cells were seeded in 24-well microplates at a density of $3 \times 10^4$ cells per well for 24 h. Then the medium was removed and healthy RA cells were added at a density of $1 \times 10^4$ cells per well. These two kinds of cells were co-cultured for another 24 h. Different DOX-loaded micelles were incubated with the co-cultured cells for 1 h. Then the cells were rinsed with PBS and fixed with 4% paraformaldehyde for 15 min, after which the medium was changed to PBS. Finally, the cells were examined under a confocal microscope.

### 2.9. Orthotopic animal models

Orthotopic glioma-bearing models were constructed using nude mice with the body weight between 20–24 g. Nude mice were purchased from Shanghai Laboratory Animal Center and maintained under standard conditions. Briefly, U251 cells ($5 \times 10^5$) were slowly implanted into the right striatum (1.8 mm lateral to the bregma and 3 mm of depth) using a stereotactic fixation device with a mouse adaptor. After surgery, mice were further maintained under standard housing conditions. Animals were maintained in accordance with the guidelines of National Laboratory Animal Welfare and Ethics, China, and approved by the ethics committee of Fudan University.

### 2.10. Targeting evaluation *in vivo*

Tissue distribution was carried out to evaluate the targeting efficiency of micelles *in vivo*. The near infrared dye, ICG, was loaded to micelles to avoid the disturbance of autofluorescence. ICG-loaded micelles (250 μg calculated DOX per mouse) modified with normal or scrambled $I_6P_8$ peptide were intravenously administrated to the glioma-bearing mice. After 4 h, the mice were sacrificed and major organs (brain, heart, liver, spleen, lung and kidney) were excised. Fluorescent imaging analysis was performed using an In Vivo IVIS Spectrum Imaging System (PerkinElmer, U.S.A.).

 

### 2.11. Anti-glioma effects

TUNEL apoptosis detection and survival analysis were applied to evaluate the anti-glioma effects. At the $10^{th}$, $12^{th}$ and $14^{th}$ day after surgery described above, glioma-bearing mice were intravenously injected with saline (the negative control), free DOX (the positive control, 250 μg per mouse), $I_6P_8$scr-D-M and $I_6P_8$-D-M at the dose of 250 μg calculated DOX per mouse. Another positive control was TMZ-treated group, in which mice received TMZ *via* intragastric administration with a dose of 50 mg $kg^{-1}$ at the $10^{th}$, $11^{th}$, $12^{th}$, $13^{th}$ and $14^{th}$ day after surgery. Two days later, two mice from each group were sacrificed and used for preparing frozen sections (10 μm). Slides were stained with DAPI and then examined using TUNEL apoptosis detection kit (FITC-labeled) according to the manufacturer's instruction. Finally, all the treated slides were observed under a fluorescent microscope. Ten mice from each group were continually monitored for survival.

### 2.12. Data analysis

Data were expressed as mean ± S.D. Statistical analysis was performed by two-tailed student's *t*-test using GraphPad InStat 3. Statistical significance was defined as $p < 0.05$. The survival data were analyzed by GraphPad Prism 5 using the Kaplan-Meier method and the log-rank test.

## 3. Results and discussion

### 3.1. Synthesis and characterization of polymers

The successful conjugation of the multifunctional $I_6P_8$ or the scrambled peptide ($I_6P_8$scr) to the classical PEG–PLGA polymer was based on the specific reaction between –SH group on peptides and –Mal group on PEG, which was consequently evidenced by the NMR results. As shown in Fig. S1,† the characteristic peak of –Mal around 6.7 ppm in the original Mal–PEG–PLGA micelles disappeared after conjugation with peptides, demonstrating the covalent bonding of $I_6P_8$ or $I_6P_8$scr with PEG–PLGA. Other peaks, indexed as the repeat units of PEG at 3.6 ppm and the typical methyl/methylene chemical shifts in lactide units (1.6 ppm & 5.2 ppm) and glycolide units (4.8 ppm) of PLGA, all reserved, which proved the no other special bonding and the stability of the multifunctional micelle polymers.

### 3.2. Characterizations of prepared micelles

According to the above procedure, different amounts of peptides were conjugated to PEG–PLGA to form $I_6P_8$–PEG–PLGA micelle. As shown in Table 1, all these micelles were around 24 nm with excellent polydispersity. Anti-cancer drug, DOX, could be encapsulated in these micelles. The encapsulation and loading efficiency slightly went up when increasing the amount of peptide ligands. This might be attributed to the increased hydrophilic segment in polymer, which can stabilize the micelles with even more hydrophobic segment (DOX) aggregated together *via* surface hydration layer, in good agreement with the results in Luo's lab.[23] However, this effect reached a platform, indicating that proper amount of the peptide ligand might achieve suitable encapsulation and loading efficiency. Then, three different micelle formulations were characterized. The results showed that no apparent difference was observed in size, encapsulation and loading efficiency (Table 2). Furthermore, the cumulative DOX release from these three micelles was also similar (Fig. S2†), suggesting the parallel preparations of micelles.

### 3.3. Cellular uptake

The optimal amount of $I_6P_8$ peptide conjugated to PEG–PLGA was screened *via* cellular uptake qualified by confocal microscopy and quantified by intracellular DOX level. As shown in Fig. 1A–L, the cellular uptake of $I_6P_8$-D-M increased with the molar percent of $I_6P_8$–PEG–PLGA and then reached a platform. When the molar percent was 5%, the cells showed strongest DOX signal. This was verified by the quantified result where the 5% molar percent of $I_6P_8$ mediated the highest cellular uptake of $I_6P_8$-D-M compared to other groups ranged from 0–40% (Fig. 1M). It has been reported that optimal modification extent of targeting ligands might introduce maximum cellular uptake.[21] In this work, the optimal molar percent of $I_6P_8$ in the micelles was 5%, which was therefore fixed for the preparation of $I_6P_8$-D-M in the following experiments.

### 3.4. Transportation across the BBB

The BBB-crossing ability of different micelles was evaluated in *in vitro* BBB monolayers. With the modification of $I_6P_8$ peptide, the significantly enhanced permeability and transport ratio of micelles were observed from the comparison results (Fig. 2). The apparent permeability of $I_6P_8$-D-M was $13 \times 10^{-6}$ cm $s^{-1}$ after 1 h incubation, while those of $I_6P_8$scr-D-M and D-M were only $4.26 \times 10^{-6}$ cm $s^{-1}$ and $3.82 \times 10^{-6}$ cm $s^{-1}$, respectively. No apparent difference in BBB transportation was observed between the two control groups. These results verified the IL-6 receptor-mediated transportation, and also $I_6P_8$ peptide was an important segment in mediating micelles across the BBB.

Table 1 Characteristics of $I_6P_8$-D-M with different molar percent of $I_6P_8$–PEG–PLGA (mean ± S.D., $n = 4$)

| Molar percent of $I_6P_8$–PEG–PLGA | Micellar size (nm) | Polydispersity | EE (%) | LC (%) |
|---|---|---|---|---|
| 2.5% | 23.08 ± 1.01 | 0.101 ± 0.02 | 89.2 ± 1.7 | 28.0 ± 0.8 |
| 5% | 24.11 ± 1.36 | 0.121 ± 0.02 | 90.1 ± 1.3 | 30.1 ± 0.6 |
| 10% | 23.55 ± 1.47 | 0.075 ± 0.01 | 91.0 ± 2.3 | 30.3 ± 0.9 |
| 20% | 23.89 ± 1.08 | 0.162 ± 0.09 | 91.7 ± 1.9 | 31.0 ± 0.7 |
| 40% | 25.21 ± 1.91 | 0.176 ± 0.11 | 90.1 ± 1.6 | 30.2 ± 0.9 |

Table 2 Characteristics of different DOX-loaded micelles (5% molar percent of peptide in modified micelles) (mean ± S.D., $n = 4$)

| Polymeric micelles | Micellar size (nm) | Polydispersity | EE (%) | LC (%) |
|---|---|---|---|---|
| D-M | 23.16 ± 0.95 | 0.090 ± 0.01 | 88.9 ± 1.6 | 28.8 ± 0.6 |
| $I_6P_8$scr-D-M | 24.53 ± 1.52 | 0.108 ± 0.02 | 90.7 ± 2.7 | 30.6 ± 0.9 |
| $I_6P_8$-D-M | 24.11 ± 1.36 | 0.121 ± 0.02 | 90.1 ± 1.3 | 30.1 ± 0.6 |

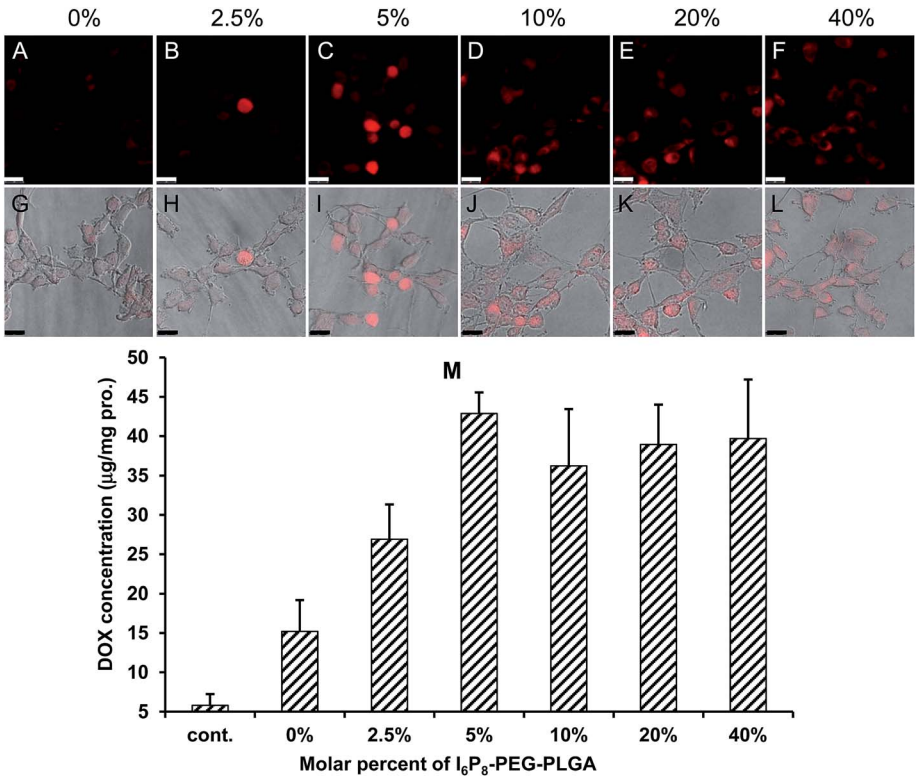


Fig. 1 Confocal microscopy images (A–L) and intracellular DOX level (M) of $I_6P_8$-D-M with different molar percent of $I_6P_8$–PEG–PLGA. The micelles were incubated with U251 glioma cells for 1 h. Red: DOX. Bar = 25 μm. Data were represented as mean ± S.D. ($n = 4$).

### 3.5. Glioma-targeted efficiency

Glioma-targeted efficiency of different drug-loaded micelles was determined in the co-culture model of GFP-U251 glioma cells and RA normal brain cells. In $I_6P_8$-D-M-treated wells, much stronger DOX signal was observed in U251 cells compared to that in RA cells (Fig. 3K–O). In contrast, in D-M and $I_6P_8$scr-D-M-treated wells, all the DOX signals were weak and had no apparent difference between U251 and RA cells (Fig. 3A–J). This demonstrated the efficient targeting ability of $I_6P_8$-D-M to glioma cells. In view of the no distinguished difference between D-M and $I_6P_8$scr-D-M in BBB-crossing and glioma-targeted efficiency, only $I_6P_8$scr-D-M was applied as the control in the following studies.

### 3.6. *In vivo* targeting evaluation

The *in vivo* targeting ability of micelles was studied by the fluorescence imaging of mice intravenously injected with ICG-loaded micelles, which could achieve strong and accurate signals without disturbance of animal autofluorescence. As shown in Fig. 4A, the $I_6P_8$-modified micelle mediated much more intensive accumulation within glioma area, compared to that of $I_6P_8$scr-D-M. Interestingly, apparent accumulation of $I_6P_8$-D-M was observed around the central glioma area, which might be the glioma stem cells. It has been reported that IL-6 signal pathway is important not only in glioma cells but also in glioma stem cells.[20,24] Thus this work further indicated the desirable accumulation of $I_6P_8$-D-M within both glioma cells and glioma stem cells, which can therefore be exploited as brain drug delivery systems for recurrent glioma therapy. Moreover, $I_6P_8$-D-M treated mouse exhibited less liver fluorescence than the $I_6P_8$scr-D-M treated one (Fig. 4B), revealing the relatively low nonspecific retention of $I_6P_8$-D-M *in vivo*. Interestingly, large amount of accumulation within liver and kidney was observed for both micelles, indicating the possible excretion by these two organs (Fig. 4B). However, this exists inconsistency compared to a previous study where more micelles were found in the liver

 

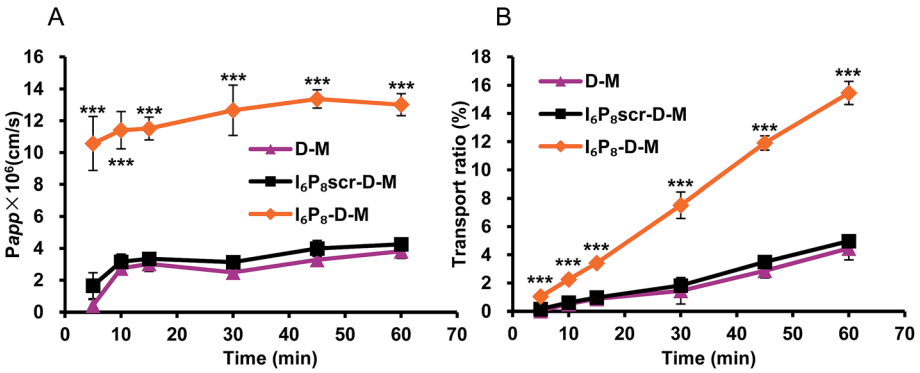


Fig. 2 The apparent permeability and transport ratio of different micelles across the *in vitro* BBB monolayers. Data were represented as mean ± S.D. ($n = 4$). Significance: ***, $p < 0.001$.

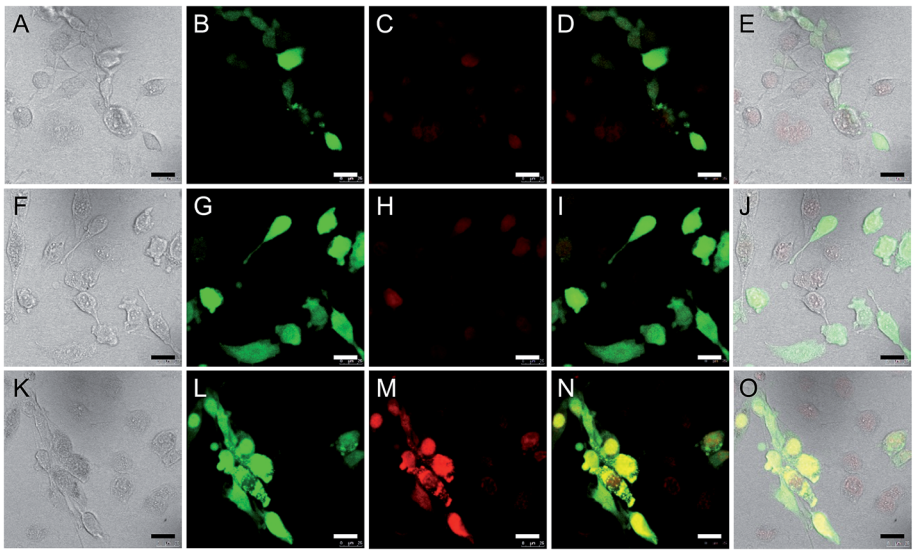


Fig. 3 *In vitro* glioma-targeted efficiency of D-M (A–E), $I_6P_8$scr-D-M (F–J) and $I_6P_8$-D-M (K–O). The micelles were incubated with the co-culture model of GFP-U251 glioma cells and RA normal cells for 1 h. Red: DOX. Green: GFP-labled U251 cells. Bar = 25 μm.

and spleen,[21] the reason of which should be further explored in the future study.

### 3.7. Glioma apoptosis

*In vivo* anti-glioma effect of different formulations was firstly evaluated using TUNEL apoptosis detection kit, with free DOX and commercial TMZ as positive controls, and saline as the negative control. As shown in Fig. 5, owing to the only EPR effect of DOX-loaded formulations, the glioma apoptosis of $I_6P_8$scr-D-M treated mouse was just a little more than that of free DOX group. The $I_6P_8$-D-M treated mouse exhibited highest glioma apoptosis among all the groups, even higher than the commercial TMZ treated group. This evidenced the strongly targeting lethal effect of $I_6P_8$-D-M for glioma therapy.

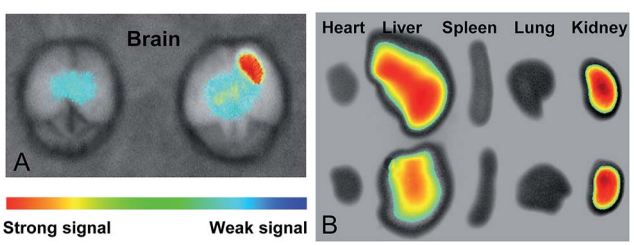


Fig. 4 Fluorescent images of main organs of glioma-bearing nude mice treated with ICG-loaded $I_6P_8$scr-modified micelle (left in A and up in B) and $I_6P_8$-modified micelle (right in A and down in B). The organs were excised 4 h after treatments. The fluorescence signal of near-infrared dye ICG was recorded.

### 3.8. Survival analysis

*In vivo* anti-glioma effect was secondly verified *via* the survival profile. As shown in Fig. 6, an apparently prolonged survival time was observed in $I_6P_8$-D-M treated mice (49.5 days) as compared to those treated with saline (31 days), free DOX (33.5 days), TMZ (44 days) and $I_6P_8$scr-D-M (36.5 days), respectively. Besides the chemotherapeutic effect, this might be attributed to (1) $I_6P_8$ peptide mediated the significantly enhanced BBB-crossing efficiency (Fig. 2) and glioma-targeted accumulation (Fig. 3 and 4), and (2) $I_6P_8$ peptide mediated the tumor growth

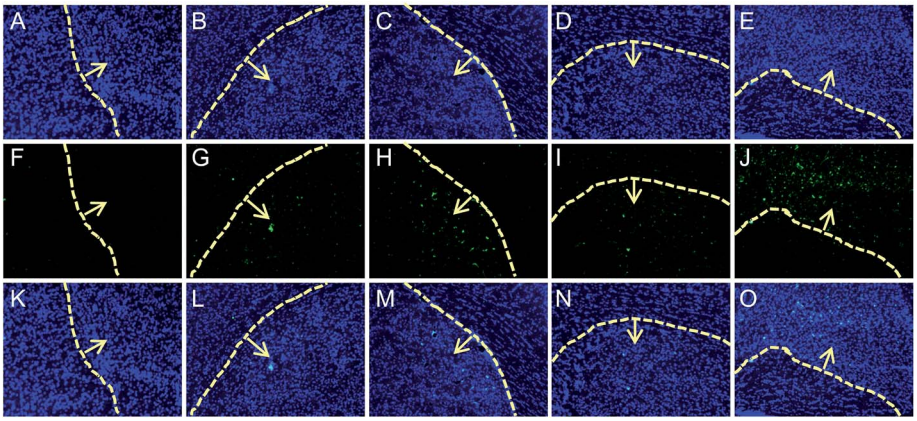


Fig. 5 Apoptosis of glioma-bearing mice treated with saline (A, F and K), free DOX (B, G and L), TMZ (C, H and M), $I_6P_8$scr-D-M (D, I and N) and $I_6P_8$-D-M (E, J and O). Slides were subjected to TUNEL apoptosis detection kit. Yellow dotted lines marked the borders of glioma and arrows pointed to the inner sides of glioma. The third panel images were merged images of corresponding first and second panels. Blue: DAPI; green: FITC-indicated apoptosis.

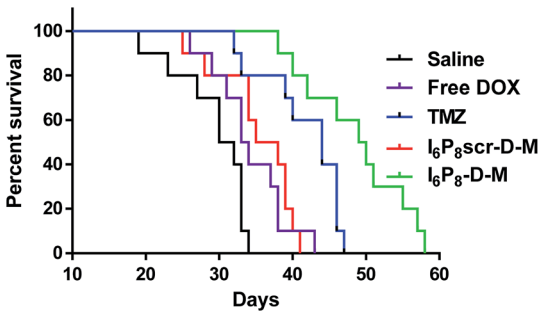


Fig. 6 The survival profile of glioma-bearing mice with different treatments.

inhibition by blocking the inimical interaction between IL-6 and IL-6R.[18,19] All the results demonstrated that multifunctional $I_6P_8$ peptide-linked classical PEG–PLGA micelle is a highly efficient glioma-targeted therapeutic platform.

## 4. Conclusions

In summary, a multifunctional $I_6P_8$ peptide-conjugated classical PEG–PLGA micelle, was prepared and developed as a drug vehicle for targeting delivery of hydrophobic DOX to glioma. The $I_6P_8$ peptide-linked micelle could significantly enhance the BBB-transporting efficiency and glioma-targeted accumulation. When encapsulating DOX, $I_6P_8$-D-M introduced highest glioma tissue apoptosis and longest survival of glioma-bearing mice, compared to other groups. Overcoming the BBB for glioma-targeted therapy accomplished by the IL-6R-mediated micelle, together with the potential tumor growth inhibition effect of $I_6P_8$ peptide, is therefore expected to be a promising alternation for brain cancer treatment.

## Acknowledgements

This study was supported by the grants from National Natural Science Foundation of China (21675032) and Nantong Municipal Science and Technology People's Livelihood Demonstration Project (MS32015023).

## References

1 N. Schleich, C. Po, D. Jacobs, B. Ucakar, B. Gallez, F. Danhier and V. Preat, *J. Controlled Release*, 2014, **194**, 82–91.
2 E. J. Chung, Y. Cheng, R. Morshed, K. Nord, Y. Han, M. L. Wegscheid, B. Auffinger, D. A. Wainwright, M. S. Lesniak and M. V. Tirrell, *Biomaterials*, 2014, **35**, 1249–1256.
3 Y. Liu and W. Lu, *Expert Opin. Drug Delivery*, 2012, **9**, 671–686.
4 A. Gutkin, Z. R. Cohen and D. Peer, *Expert Opin. Drug Delivery*, 2016, **13**, 1573–1582.
5 Y. Huang, W. Liu, F. Gao, X. Fang and Y. Chen, *Int. J. Nanomed.*, 2016, **11**, 1629–1641.
6 X. Chen, L. Tai, J. Gao, J. Qian, M. Zhang, B. Li, C. Xie, L. Lu, W. Lu and W. Lu, *J. Controlled Release*, 2015, **218**, 29–35.
7 B. Oller-Salvia, M. Sanchez-Navarro, E. Giralt and M. Teixido, *Chem. Soc. Rev.*, 2016, **45**, 4690–4707.
8 A. Jain, A. Jain, N. K. Garg, R. K. Tyagi, B. Singh, O. P. Katare, T. J. Webster and V. Soni, *Acta Biomater.*, 2015, **24**, 140–151.
9 Y. Z. Zhao, L. J. Chen, Q. Lin, J. Cai, W. Z. Yu, Y. P. Zhao, C. Y. Xu, K. L. Mao, F. R. Tian, W. F. Li, H. L. Wong and C. T. Lu, *Oncotarget*, 2015, DOI: 10.18632/oncotarget.5144.
10 Y. Z. Zhao, Q. Lin, H. L. Wong, X. T. Shen, W. Yang, H. L. Xu, K. L. Mao, F. R. Tian, J. J. Yang, J. Xu, J. Xiao and C. T. Lu, *J. Controlled Release*, 2016, **224**, 112–125.
11 R. K. Oberoi, K. E. Parrish, T. T. Sio, R. K. Mittapalli, W. F. Elmquist and J. N. Sarkaria, *Neuro-Oncology*, 2016, **18**, 27–36.
12 C. H. Fan, C. Y. Ting, Y. C. Chang, K. C. Wei, H. L. Liu and C. K. Yeh, *Acta Biomater.*, 2015, **15**, 89–101.
13 H. Yao, K. Wang, Y. Wang, S. Wang, J. Li, J. Lou, L. Ye, X. Yan, W. Lu and R. Huang, *Biomaterials*, 2015, **37**, 345–352.
14 T. Yin, L. Yang, Y. Liu, X. Zhou, J. Sun and J. Liu, *Acta Biomater.*, 2015, **25**, 172–183.

15 P. J. Yue, L. He, S. W. Qiu, Y. Li, Y. J. Liao, X. P. Li, D. Xie and Y. Peng, *Mol. Cancer*, 2014, **13**, 191.
16 X. Wei, J. Gao, C. Zhan, C. Xie, Z. Chai, D. Ran, M. Ying, P. Zheng and W. Lu, *J. Controlled Release*, 2015, **218**, 13–21.
17 T. Zong, L. Mei, H. Gao, K. Shi, J. Chen, Y. Wang, Q. Zhang, Y. Yang and Q. He, *J. Pharm. Sci.*, 2014, **103**, 3891–3901.
18 A. Sturzu and S. Heckl, *Chem. Biol. Drug Des.*, 2010, **75**, 369–374.
19 J. L. Su, K. P. Lai, C. A. Chen, C. Y. Yang, P. S. Chen, C. C. Chang, C. H. Chou, C. L. Hu, M. L. Kuo, C. Y. Hsieh and L. H. Wei, *Cancer Res.*, 2005, **65**, 4827–4835.
20 H. Wang, J. D. Lathia, Q. Wu, J. Wang, Z. Li, J. M. Heddleston, C. E. Eyler, J. Elderbroom, J. Gallagher, J. Schuschu, J. MacSwords, Y. Cao, R. E. McLendon, X. F. Wang, A. B. Hjelmeland and J. N. Rich, *Stem Cells*, 2009, **27**, 2393–2404.
21 Y. Meng, S. Wang, C. Li, M. Qian, Y. Zheng, X. Yan and R. Huang, *Int. J. Pharm.*, 2016, **498**, 40–48.
22 R. Q. Huang, Y. H. Qu, W. L. Ke, J. H. Zhu, Y. Y. Pei and C. Jiang, *FASEB J.*, 2007, **21**, 1117–1125.
23 F. Cheng, X. Guan, H. Cao, T. Su, J. Cao, Y. Chen, M. Cai, B. He, Z. Gu and X. Luo, *Int. J. Pharm.*, 2015, **492**, 152–160.
24 A. Hossain, J. Gumin, F. Gao, J. Figueroa, N. Shinojima, T. Takezaki, W. Priebe, D. Villarreal, S. G. Kang, C. Joyce, E. Sulman, Q. Wang, F. C. Marini, M. Andreeff, H. Colman and F. F. Lang, *Stem Cells*, 2015, **33**, 2400–2415.